International Journal of Earth Sciences (2021) 110:2057–2064
https://doi.org/10.1007/s00531-021-02057-1

ORIGINAL PAPER

# Relationship between channel flow initiation and crustal viscosity in convergent settings: an analog modeling approach

**Jacqueline E. Reber[1] · Chanel Smita Vidal[1] · Shae McLafferty[1] · Soumyajit Mukherjee[2]**

Received: 4 December 2020 / Accepted: 23 May 2021 / Published online: 3 June 2021


**Abstract**
Channel flow has been proposed as a mechanism to explain the formation of the Greater Himalayan Sequence that is bounded by normal sense ductile shear along the Himalayan orogen. The key requirements for channel flow are: (i) extruding middle-to-lower crust of low viscosity, and (ii) excess gravitational potential due to topography. We present scaled two-layer physical models where the effect of the gravitational potential with respect to the plate convergence rate is investigated. Viscous middle crust starts moving towards the surface where the strain rate imposed by the convergence is 30% of that arising from the lateral pressure gradient. How efficiently the low-viscosity crust extrudes is directly linked to the imposed pressure gradient. A simple correlation between the extruding rock's viscosity, the convergence rate, and the topography imposing the pressure gradient is established. The upward motion of viscous material is expected already for a mid-crustal viscosity of $10^{21}$ Pa s. This is significantly higher than previously expected, suggesting that one of the fundamental requirements for channel flow might not be necessary.

**Keywords** Channel flow · Analog experiments · Excess topography · Crustal viscosity · Himalaya · Tibetan plateau

## Introduction

The Himalayan orogen originated due to the continent–continent collision of India and Asia since ~ 54 Ma (Najman et al. 2017). Its present-day structure is dominated by several large-scale north/northeast-dipping fore–fault zones bounding different lithologic units. Three of these first-order large-scale fault structures (towards north, Main Frontal Thrust, Main Boundary Thrust, and Main Central Thrust) show a reverse sense of slip along their fault and shear zones. The forth structure, the South Tibetan Detachment System (STDS) shows a normal sense of slip with a history of compressional shear (Kellett et al. 2019) (Fig. 1A). This normal fault system has been widely documented in the field (e.g., Burg and Chen 1984; Mukherjee 2013; Mukherjee and Koyi 2010) and contains a combination of brittle and ductile features accumulating a displacement of > 35 km (Burchfiel 1992) and possibly as much as 100–200 km (Searle et al. 2003). In addition, the formation and growth of the Tibetan plateau with 5000 m of average elevation is tectonically linked to the evolution of the Himalaya (Fielding et al. 1994).

Based on geochronologic dating, the timing of motion on the STDS partially overlaps with that of the Main Central Thrust (MCT), the northernmost large-scale reverse fault (Hodges et al. 1992; Martin 2017). Both structures activated simultaneously for at least 1–2 Ma (Godin et al. 2006), with some coeval motion on a few strands for 10 Ma (Kellett et al. 2013).

Several hypotheses have been suggested to explain the formation of the STDS in a converging setting (Kellett et al. 2019). We refer to Kellett et al. (2019) and Yin (2006) for detailed reviews on the STDS. Here, we focus on channel flow as the potential mechanism for the development of the STDS (Godin et al. 2006; Grujic et al. 2011; Harris 2007; Searle et al. 2009). The channel flow model presumes: (i) a low-viscosity mid-to-lower-crust, (ii) a lateral pressure gradient due to excess topography (Beaumont et al. 2001), and (iii) coeval compressional slip of the MCT and extensional slip of the STDS. In a system where subduction and convergent plate motion are the dominant driving mechanisms the

✉ Jacqueline E. Reber
jreber@iastate.edu

[1] Department of Geological and Atmospheric Sciences, Iowa State University, Ames, IA 50011, USA

[2] Department of Earth Sciences, Indian Institute of Technology Bombay, Powai, Mumbai, Maharashtra 400076, India

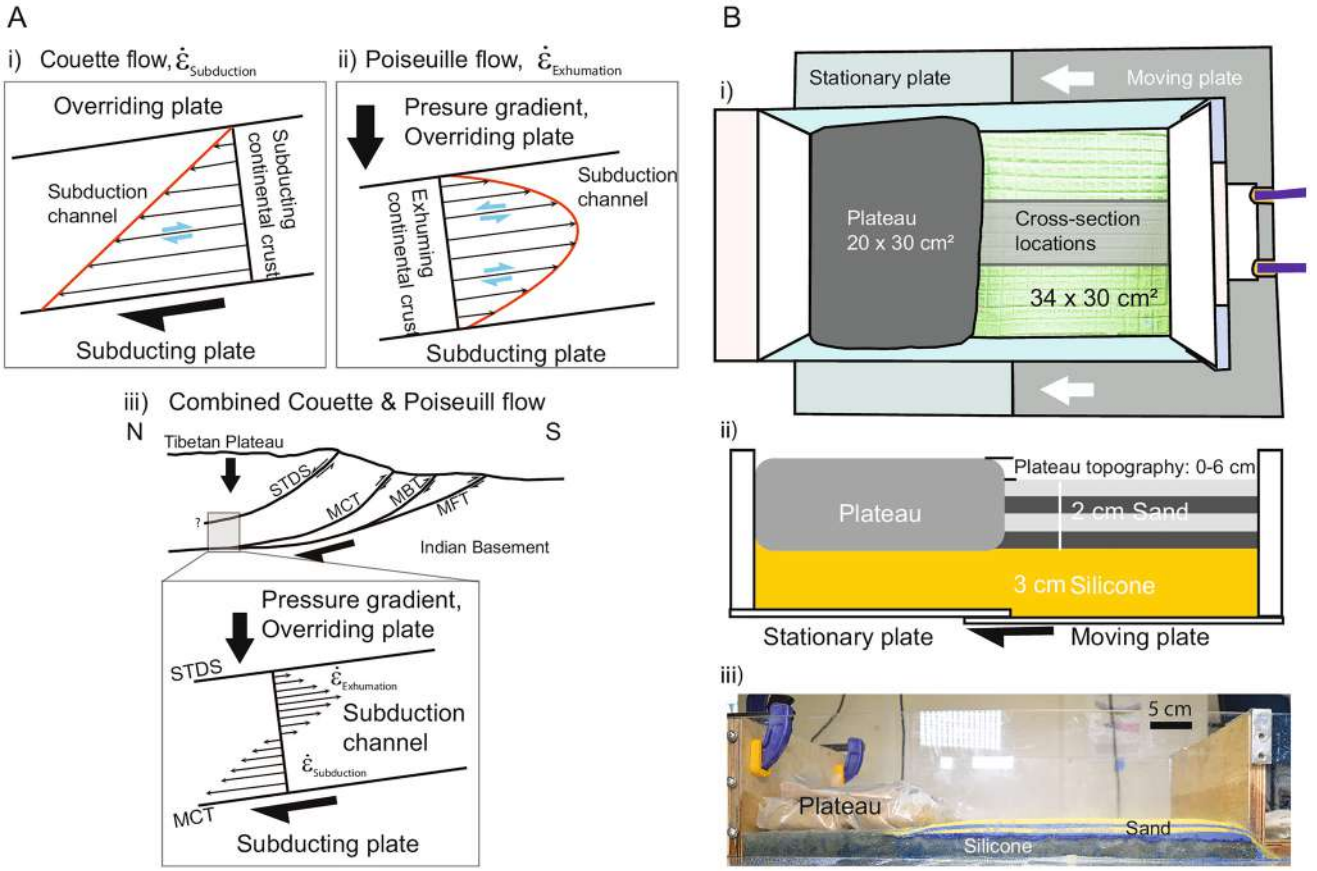


**Fig. 1** **A** (i) Subduction-related flow. (ii) Flow field for channel flow-related exhumation. (iii) Himalayan orogen illustrating the main structures (*MFT* Main Frontal Thrust, *MBT* Main Boundary Thrust, *MCT* main central thrust, *STDS* South Tibetan Detachment System. Inset: flow imposed by combined Couette and Poiseuille flow, adapted from Godin et al. (2006). **B** (i) Top-view of experimental setup. The moving plate converges with a velocity of 0.0016 $cm^{-1}$ beneath the stationary plate. (ii) Side-view of the experiment, (iii) side-view photograph of experiment

plate motion leads to Couette flow. In this flow regime the motion is driven by the subducting plate leading to crustal material being moved downward along the subduction channel (Fig. 1Ai). The expected flow regime in a system dominated by a pressure gradient imposed by the overriding plate can be described by Poiseuille or pipe flow (Fig. 1Aii). In this case, crustal material can migrate upward along the subduction channel. In the case of the Himalayan collision zone, both flow regimes are expected; Couette flow driven by the subducting plate and Poiseuille flow as a result of the pressure gradient caused by the overburden of the Tibetan plateau (Schmalholz et al. 2019). The development of channel flow depends critically on the magnitude of the strain rates governing the respective flow fields and would only be expected in situations where the strain rate of the Poiseuille flow is larger than the strain rate of Couette flow (Godin et al. 2006; Mukherjee et al. 2012). Here, we investigate the impact of the gravitational potential energy and a constant convergence rate on the flow and mobility of the viscous crust in simple, two-layer physical 1 g experiments.

## Experiments

We investigate the development of channel flow in a physical model using a two-layer sand-box setup. A 3 cm thick linear viscous polydimethylsiloxane layer (Dow Corning PDMS-DC SGM36, referred to as silicone) represents the viscous middle crust, while a 2 cm thick sand layer is used to simulate the brittle upper crust (Fig. 1B). The upper brittle crust follows a Coulomb–frictional behavior while the middle crust deforms linearly viscous. Four differently sized plateaus are constructed of rectangular $20 \times 30$ $cm^2$ packages of sand wrapped in plastic that accommodate only minimal internal deformation. The total plateau thicknesses are 2, 2.4, 2.8 and 8 cm leading to an excess topographic height of 0, 0.4, 0.8 and 6 cm, respectively.

## Scaling and model material properties

Since the models investigate a crustal-scale process in a natural gravity field, gravitational force is considered. To scale the models, all quantities with dimensions of stress are scaled down with the same factor as the linear dimensions (e.g., Davy and Cobbold 1988). We assume a 12 km thick upper continental crust (Li et al. 2006) and total crustal thickness of 30 km for the Indian plate (Makris et al. 2001), leading to a length-scale factor of $1.6 \times 10^{-6}$ (1 cm in model = 6 km in prototype). Using this length-scale, cohesion in the brittle upper crust after scaling becomes negligible. Internal friction on the other hand, is a dimensionless number and is taken to be identical in the prototype and the model (Reber et al. 2020). To fulfill this requirement, we use quartz sand with an internal friction of ~ 0.6 and a Mohr–Coulomb type frictional behavior (Byerlee 1978; Krantz 1991). The quartz sand grains are well sorted and well-rounded with an average grain size of 0.31 mm. The dyes have no impact on the mechanical behavior of the sand but act as passive markers for the deformation visualization.

The scaling of the viscous layer is dependent on strain rate where we need to consider the time scale. This scaling is largely dominated by the motor speeds available on the experimental apparatus. The slowest motor velocity we can achieve is 0.0016 cm $s^{-1}$. If we consider a plate convergence velocity of 5 cm $year^{-1}$ for the India–Asia collision (Jagoutz et al. 2015), the velocity will scale by a factor of $10^4$. Using the already established length scale we end up at a time scale of $10^{-10}$ (length scale/velocity scale). Based on this time scale the scaling factor of dynamic viscosity is $10^{-16}$ (length scale × time scale).

To fulfill the requirement of a low viscosity middle crust for channel flow we assume a middle crustal viscosity of $10^{19}$ Pa s. in nature. This is at the lower end of the range of the estimated magnitude (Huismans and Beaumont 2011) but falls within the possible range of viscosities of the Greater Himalayan Sequence rocks that extruded by channel flow (Mukherjee 2013). Applying the scaling factor for viscosity we end up with a silicone viscosity of about $10^3$ Pa s. For the pure, unaltered silicone we measure a viscosity of $3.4*10^4$ Pa s. To modify the viscosity of the silicone we mixed the pure silicone with oleic acid (Weijermars 1986). By adding oleic acid, we lower the viscosity by approximately one order of magnitude to $4*10^3$ Pa s. All viscosity measurements are taken at room temperature with a concentric viscometer (Reber et al. 2013). The silicone deforms in a linear viscous manner at experimental strain rates (Reber et al. 2013; Talbot and Aftabi 2004; ten Grotenhuis et al. 2002; Weijermars 1986).

By changing the height of the plateau in individual experiments from 0 to 6 cm, we vary the gravitational potential energy imposed by the excess topography on the viscous layer. Note, the plateau and excess topography do not evolve during an experiment, but are different between individual experiments. The first set of experiments were conducted with a plateau of the same height as the sand layers (no plateau). The only force acting in these experiments is coming from the convergence. In a second set of experiments we added 0.4 cm to the plateau height (2.4 km prototype height). In the third experiment, we scaled the elevation of the plateau to the current topography of the Tibetan plateau [~ 5 km (Zhou et al. 2014)] leading to a plateau height of 0.8 cm. Note that in experiments with plateau heights of 0.4 and 0.8 cm the total crustal thickness beneath the plateau is not scaled. In a fourth set of experiments we apply a significantly larger plateau (6 cm plateau elevation, this is corresponding to 36 km in the prototype). This plateau size does not scale to the Tibetan prototype, rather it allows us to investigate an end-member case with an extreme gravitational potential.

## Experimental setup and data acquisition

The experimental apparatus (Fig. 1B) consists of two base plates where one base plate moves at a velocity of 0.0016 cm $s^{-1}$ below a stationary second base plate. The transition between the two plates is located ~ 2 cm from the edge of the plateau simulating the subduction of the Indian plate below the Asian plate. This experimental setup is a modification of a more classic convergent setup where the model material is deformed against a stationary back-stop (e.g., Davis et al. 1983). Our experimental setup design is inspired by the Himalayan prototype where the middle/lower crust below the Tibetan plateau contributes to channel flow. The setup used in this study allows for a similar motion of the silicone, which is located below the plateau. This would not be possible with a setup where the deformation localizes directly against a fixed back-stop. The experiments are contained in a 30 cm wide and 54.5 cm long box that can accommodate shortening of up to 12 cm (72 km in prototype). All the side walls are lubricated with liquid soap to minimize friction and avoid the case of slip boundary condition.

Final deformation in each experiment is reached after ~ 42 min and documented by cross sections cut parallel to the shortening direction at a spacing of 1.5 cm (Fig. 2). To quantify surface uplift, we take ~ 40 photos of each experiment from various angles at the start of the experiment and at approximately 11 cm of shortening. These photographs are used to construct 3D point clouds. By comparing the point cloud at the beginning of an experiment to the point cloud at the end of the experiment, we can determine the surface uplift during the experiment (Fig. 3). Furthermore, top-view photographs are taken every 10 s, which are used

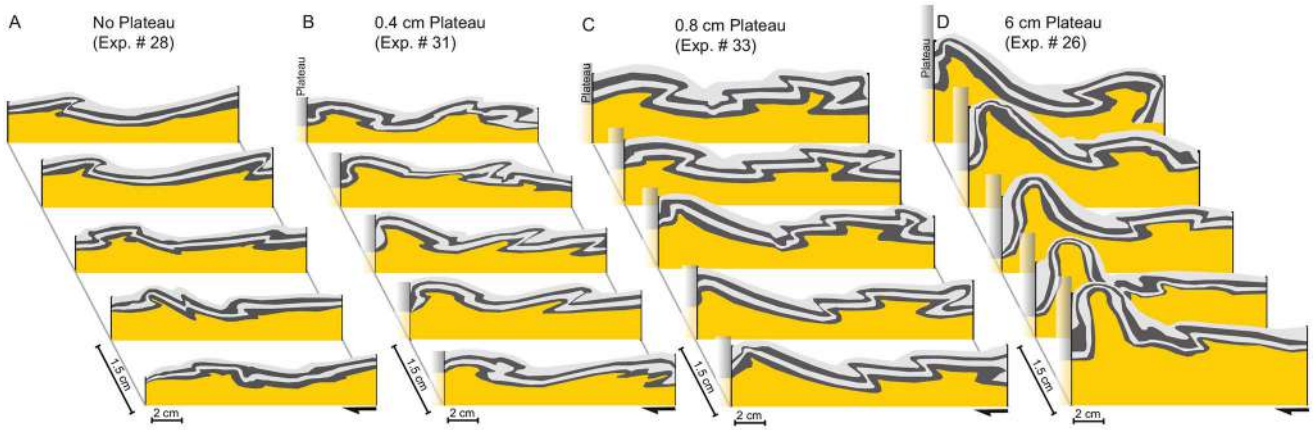


**Fig. 2** Cross sections cut parallel to the shortening direction and spaced 1.5 cm (see Fig. 1B). The cross sections show only the deformed layers; the plateau location is indicated with a shaded box to the left of each section. Sand: light and dark gray layers. Silicone: yellow. **A** Experiment without elevated plateau. **B** Small plateau with 0.4 cm topography. **C** Plateau scaled to current elevation of the Tibetan plateau, and **d** Plateau with 6 cm excess topography

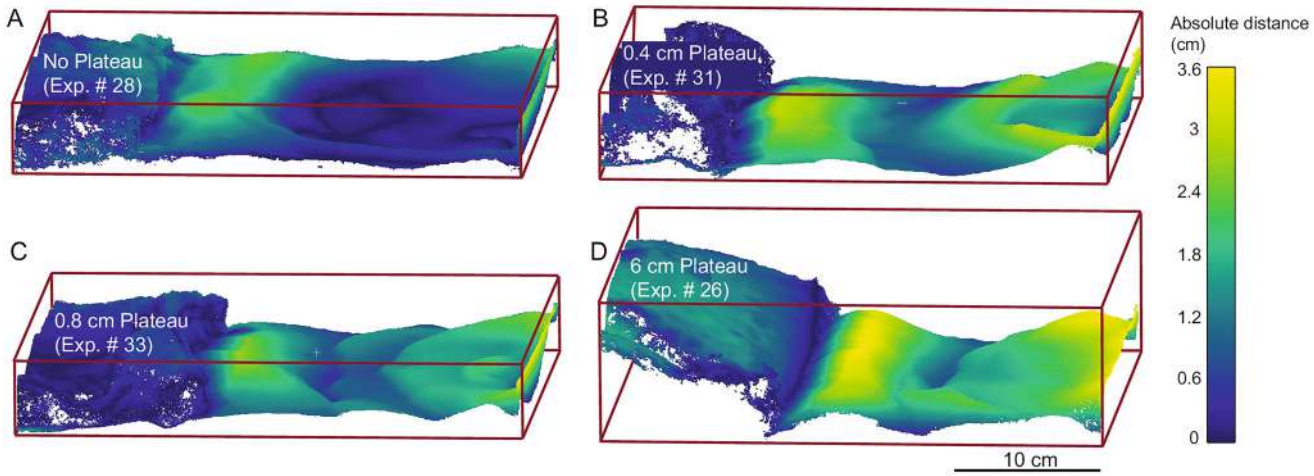


**Fig. 3** 3D surface reconstructions using Cloud Compare (version 2.9.1) and Agisoft (version 1.5.4). Colors indicate the total uplift. **A** Experiment with no plateau, **B** small plateau with 0.4 cm topography, **C** plateau (0.8 cm) scaled to current topography of the Tibetan plateau, and **D** plateau with 6 cm excess topography. Due to limited photographs around the plateaus, their 3D surfaces are not well resolved and appear larger. While the plateau in D shows no internal deformation within the plateau, in all the other experiments the plateau accommodates a small part of the shortening

to quantify the distribution of horizontal movement using Particle Image Velocimetry (Fig. 4).

## Limitations

We are using a granular, multi-colored sand layer to represent the behavior of the brittle upper crust and a viscous layer as an analog for the middle and lower crust. This is of course a strong simplification of the natural prototype that allows us to identify the impact of gravitational potential and simultaneous convergence on the mobility of the viscous material in the absence of other factors. The experiments do not take effects such as temperature, pressure, discrete fault planes, slip rates, stress distribution, or chemical reactions/metamorphism into account. While the experiments are scaled with respect to convergence velocity, viscosity, and length, they are not scaled with respect to density. The quartz sand has a density of 1.74 g $cm^{-3}$, while the silicone has a density of 1.16 g $cm^{-3}$. In the prototype, we would expect the density of the upper crust to be lower than the density of the middle crust, which is at odds with the experiments. To compensate for this discrepancy between the experiments and the prototype we conducted the experiments fast enough to avoid Rayleigh–Taylor instabilities and the spontaneous upwelling of silicone (Dooley et al. 2007;

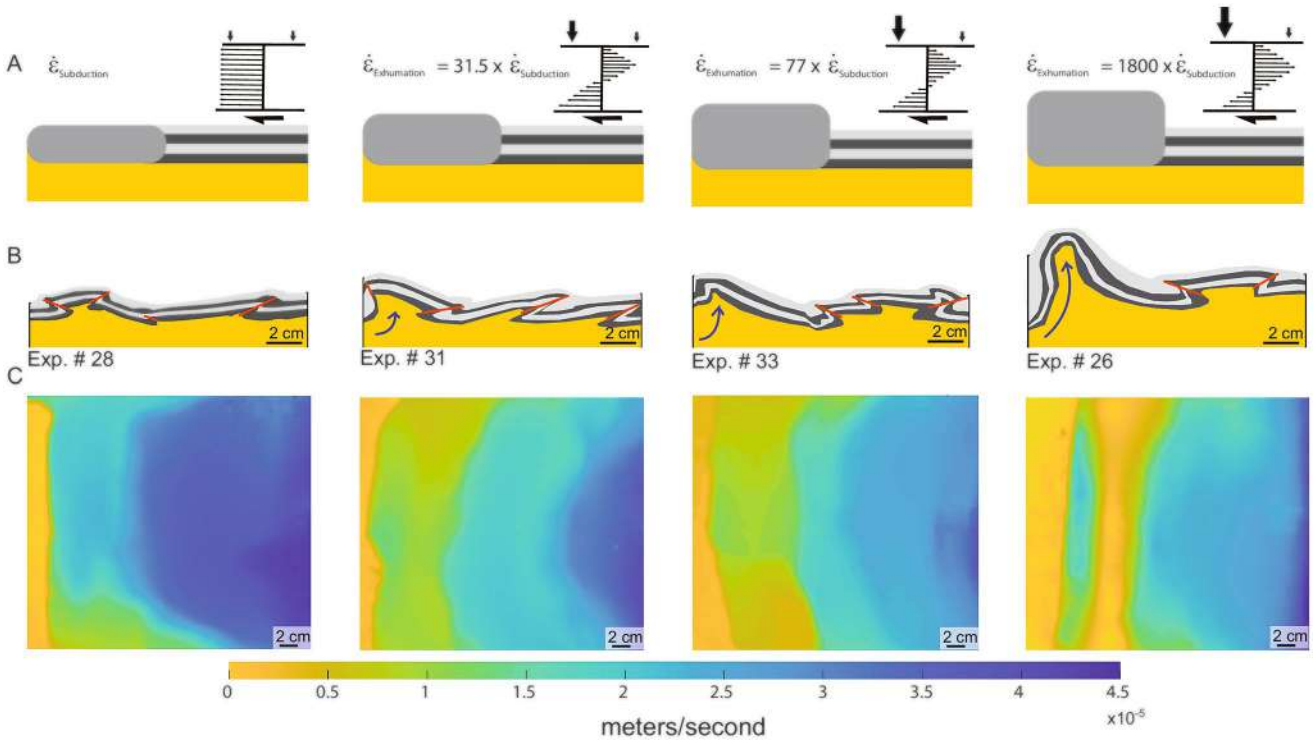


**Fig. 4** Effect of the Tibetan plateau weight on the flow in the lower crust. **A** Schematic setup of the experiment including sketches of the predicted flow fields. **B** Cross sections from experiments. Red: faults, blue: flow of silicone. **C** Particle Image Velocimetry [using PIVlab, (Thielicke and Stamhuis 2014)] of the deforming sand surface illustrating the average shortening velocity during the experiments

Vendeville and Jackson 1992). Furthermore, our experiments do not include erosion and the actual subduction of material. The topography of the Tibetan plateau in the experiment is not evolving through time and internal deformation of the plateau is minimal. This is certainly a simplification given the actual tectonics of the plateau (e.g., Spicer et al. 2003) and makes a direct comparison with the timing of the Tibetan thickening unreasonable. The motion of the subduction is simulated by the horizontal motion of one base plate beneath another base plate. The experimental setup used here has a flat base and does not allow for isostatic compensation of the topography. We are therefore only scaling for the current Tibetan plateau elevation in the experiments with a 0.8 cm thick plateau. Taking selected parameters in analog models has been standard practice. Because of these simplifications, the experiments allow us to isolate the impact of the strain rates resulting from convergence and gravitational potential on the movement of the middle crust.

## Results

A total of 12 experiments were conducted (Table 1). Experiments with different plateau sizes in combination with a constant convergence rate lead to significantly different internal structures. While the details, for instance the exact location of faults, vary between individual experiments, the overall characteristics, such as presence of faults and magnitude of uplift, were reproducible. Here, we show four representative experiments of the different plateau sizes.

To separate the impact of the plateau weight and the resulting pressure gradient on deformation, we conducted one experiment with a 6 cm high plateau in the absence of convergence. This experiment was the only one that did not exhibit any faults (Table 1, experiment #34). Experiments with no plateau but convergence show hinterland-ward and foreland-ward fore-thrusting and back-thrusting, respectively (Table 1, experiments #27 and #28). Experiments with a small plateau (0.4 cm excess topography, Table 1 experiments #29–31) show multiple thrust planes, which predominantly dip towards the hinterland, while experiments with a 0.8 (Table 1, experiments # 24–26) and 6 cm thick plateau (Table 1, experiment #23) do not show a preference in thrust plane orientation (Fig. 2). The number of faults ranges between two and five in all experiments. While in all experiments silicone moves towards the surface along fault planes, upwelling of silicone can only be observed in experiments that have a plateau, where the magnitude of the upwelling is directly related to the plateau size. The upwelling is constrained to an area parallel to the edge of the plateau.

**Table 1** Experiment parameters and resulting structures

| Exp. # | Silicone viscosity (Pa s) | Convergence rate ($s^{-1}$) | Exhumation rate ($s^{-1}$) | Excess plateau weight (g) | Plateau elevation (cm) | Experiment run time (s) | #Faults dip towards foreland | #Faults dip towards hinterland | Total #faults |
|---|---|---|---|---|---|---|---|---|---|
| 27 | 4000 | 0.00013 | 0 | 0 | 0 | 2505 | 1 | 4 | 5 |
| 28 | 4000 | 0.00013 | 0 | 0 | 0 | 2402 | 1 | 2 | 3 |
| 29 | 4000 | 0.00013 | 0.0041 | 100 | 0.4 | 2009 | 0 | 2 | 2 |
| 30 | 4000 | 0.00013 | 0.0041 | 100 | 0.4 | 1980 | 2 | 2 | 4 |
| 31 | 4000 | 0.00013 | 0.0041 | 100 | 0.4 | 2805 | 1 | 3 | 4 |
| 32 | 4000 | 0.00013 | 0.01 | 250 | 0.8 | 2664 | 1 | 3 | 4 |
| 33 | 4000 | 0.00013 | 0.01 | 250 | 0.8 | 2640 | 3 | 2 | 5 |
| 34 | 4000 | 0 | 0.245 | 7393 | 6 | 2640 | 0 | 0 | 0 |
| 26 | 4000 | 0.00013 | 0.245 | 7393 | 6 | 2820 | 1 | 1 | 2 |
| 24 | 4000 | 0.00013 | 0.245 | 7393 | 6 | 1918 | 2 | 1 | 3 |
| 25 | 4000 | 0.00013 | 0.245 | 7393 | 6 | 3172 | 2 | 2 | 4 |
| 23 | 40,000 | 0.00013 | 0.0245 | 7393 | 6 | 2396 | 2 | 2 | 4 |

While the topographic uplift is most pronounced close to the plateau and the converging sidewall, its magnitude depends on the size of the plateau (Fig. 3). The topographic uplift close to the plateau is driven by the upwelling of silicone in these locations, while the increase in topography close to the converging sidewall is a boundary effect. In the absence of a plateau we observe a maximum change in elevation of 2.4 cm due to the shortening. The experiment with the largest plateau (6 cm) shows a maximum elevation change of 3.6 cm compared to its undeformed state (Fig. 3). Both experiments with plateau thicknesses of 0.4 and 0.8 cm exhibit maximum elevation changes of 3 cm compared to the undeformed state. Quantifying the horizontal motion in the experiment shows that it is fastest close to the converging sidewall with $4.5*10^{-5}$ $ms^{-1}$ and tends to zero at the plateau (Fig. 4). While this decrease in horizontal velocity is expected, the decrease is not gradual but separated into areas of equal velocity bound by faults reaching the experimental surface (Fig. 4). Experiments with a plateau show an extended area of reduced horizontal motion when compared to the experiment with no plateau. These areas are correlated to locations of upwelling of silicone. The most extreme case can be observed in the experiment with a 6 cm thick plateau, where no horizontal motion of the strongly uplifted parts can be detected (Fig. 4).

## Discussion

Our experiments show a clear correlation between the excess topography and the mobility of the viscous layer. They show that already with a modestly sized plateau (0.4 cm excess topography) features characteristic for channel flow can be observed (Fig. 4). While the additional load of the plateau moves viscous silicone towards the surface, we do not see it outcropping at the surface. The reason for this is the absence of any localized denudation processes in the models. While denudation is necessary to expose mid crustal material at the surface (Beaumont et al. 2004), our experiments show that denudation is not necessary to drive the upwelling, similar to previous analog channel flow models conducted in a different context (Mukherjee et al. 2012). In those experiments, a Poiseuille flow developed solely by producing a pressure difference without any denudation simulating the extrusion of the Greater Himalayan Crystallines, the terrain within the MCT and STDS. Because of the lack of denudation, our models resemble findings by Beaumont et al. (2004), where they investigate exhumation of middle crustal material due to channel flow with sufficient and insufficient denudation. Similar to their findings, we observe the formation of folds and plug-like structures in the absence of denudation. But in contrast to their results, we observe a progressive movement of the channel towards the surface also in the absence of denudation. Beaumont et al. (2004) did not address how the Tibetan topography alone can govern crustal channel flow in the Himalaya. Our experiments do not model the continuous development and detailed structures of the Tibetan plateau. Rather, we are investigating four specific scenarios of various amounts of excess topography. Spicer et al. (2003) argue that the Tibetan plateau reached its current elevation 15 Ma ago. This coincides with the dated extensional shear along the STDS coeval to the MCT's compressional shear leading to channel flow (Godin et al. 2006) and suggests that channel flow initiated after the rise of the Tibetan plateau.

Our experiments utilize a horizontal middle crustal layer where the total thickness is not scaled to nature. This is in contrast to processes in nature, where part of the topography would be compensated with deeper roots following the Airy

isostasy model (Mukherjee 2017). This inherently leads to a topography that is exaggerated compared to that expected in nature (for example uplift of 3 cm = 18 km). Furthermore, our models do not consider erosion, which is an additional factor that leads to an exaggerated topography change.

To compare the effect of convergence versus excess topography we calculate the convergence rate and silicone exhumation rates. The convergence rate is simply obtained by dividing the motor velocity by the shortening distance (Table 1). The exhumation rate is approximated using a simple flow law for linear viscous fluids:

$$\dot{\varepsilon}_{\text{Exhumation}} = \frac{\sigma}{\eta}, \tag{1}$$

where $\eta$ is the measured silicone viscosity and $\sigma$ is the stress imposed by the plateau calculated from its mass (kg), area ($m^2$), and gravitational acceleration ($ms^{-2}$).

The models illustrate that there is a fine balance between the convergence rate and the gravitational potential energy, which governs the dominant flow fields. Mandal et al. (2015) have investigated the impact of the convergence velocity on the development of the topography of the Himalaya and Tibet by systematically changing the under-thrusting velocity within 2–8 cm $year^{-1}$ in a one-layer numerical model. They found that channel flow can develop in cases of low convergence velocities and gravitational collapse. We are using a low and constant convergence rate in our experiments and find similar results, despite using a layered model. In the absence of excess topography and therefore pressure gradient, no motion of the silicone is observed. Already in the presence of a small plateau with 0.4 cm of excess topography, silicone moves toward the surface. We interpret this mobility of the viscous layer as one of the key requirements of channel flow and initiation thereof. In this experiment the convergence rate is approximately 30% of the strain rate resulting from the excess gravitational potential (Table 1). Plateaus imposing larger gravitational potentials lead to an increase in the mobility of the viscous layer. This direct link between the plateau elevation and the upward movement of the viscous middle crust can be used to investigate the maximum middle crustal viscosity where channel flow can still initiate.

Our experiments show that the minimum requirement to initiate channel flow is $\dot{\varepsilon}_{\text{Convergence}} \times 30 \approx \dot{\varepsilon}_{\text{Exhumation}}$ in a system where convergence and excess topography are driving deformation at the same time. This allows to estimate the viscosity needed to initiate channel flow in a natural setting such as the Himalaya. For this purpose, we reformulate Eq. (1) to:

$$\frac{\eta}{h} = \frac{\rho g}{\dot{\varepsilon}_{\text{Convergence}} \times 30}, \tag{2}$$

where $\eta$ is the viscosity of the middle crust and stress has been reformulated to $\sigma = \rho g h$, with $\rho$ average density of the plateau, $g$ gravitational acceleration, and $h$ elevation of the plateau.

Applying Eq. (2) to estimates from the Tibetan plateau using an average crustal rock density of 2830 $kgm^{-3}$ and a strain rate for convergence of $4*10^{-8}$ $year^{-1}$ (Hao et al. 2019) allows for an estimate of the maximum viscosity of the middle crust necessary to initiate channel flow. This back of the envelope calculation leads to a maximum viscosity of the middle crust between $1.4*10^{21}$ and $3.45*10^{21}$ Pa s, for 2–5 km of plateau topography. This is significantly higher than values previously taken for channel flow, where $\eta = 10^{18}$–$10^{19}$ Pa s. (Beaumont et al. 2001, 2004; Mandal et al. 2015) but within the limit established by Mukherjee (2013). An excess topography of 2 km could already initiate channel flow at a mid-crustal viscosity higher than previously assumed. This suggests that in the presence of a low viscosity middle crust an even smaller gravitational potential can lead to the initiation of channel flow.

## Conclusions

Channel flow has been suggested as one explanation for the co-existence of normal and reverse shear sense motion on shear zones bounding the Greater Himalayan Sequence. The two key requirements for channel flow are an extruding middle–lower-crust of low viscosity, and excess gravitational potential due to topography. We investigate the impact of excess potential energy on the formation of channel flow in physical experiments with a constant convergence rate. The results show that, where the convergence rate is approximately 30% the strain rate of exhumation, channel flow can be initiated. This indicates that a relatively small plateau can lead to the upward flow of middle crustal material. Linking estimated values of excess topography, average rock properties, and the rate of convergence or subduction for the Himalaya orogen suggests that channel flow initiates with a middle crustal viscosity higher than previously considered. This questions the requirement for a low viscosity middle crust as one of the conditions for channel flow.

**Acknowledgements** Thanks to Department of Earth and Environmental Sciences, University of Minnesota—Minneapolis for lending us the experimental apparatus. CSV received funding from the ISU LAS Dean's High Impact Undergraduate Research Award and the GEAT Undergraduate Research Grant. SMcL received funding from the GEAT Undergraduate Research Grant. SM was supported by a CPDA grant of IIT Bombay. We thank the editor Wolf-Christian Dullo for the handling of the paper and João C. Duarte and an anonymous reviewer for constructive comments. The raw data, including photographs of all experiments, can be accessed via the Iowa State University data repository (https://doi.org/10.25380/iastate.13388150).

## Declarations

**Conflict of interest** None of the contributing authors report a conflict of interest.

## References


Beaumont C, Jamieson RA, Nguyen MH, Lee B (2001) Himalayan tectonics explained by extrusion of a low-viscosity crustal channel coupled to focused surface denudation. Nature 414(6865):738–742

Beaumont C, Jamieson RA, Nguyen MH, Medvedev S (2004) Crustal channel flows: 1. Numerical models with applications to the tectonics of the Himalayan-Tibetan orogen. J Geophys Res 109(B6). https://doi.org/10.1029/2003JB002809

Burchfiel BC (1992) The South Tibetan detachment system, Himalayan Orogen. Geol Soc Am Bull, Special Papers, no. 269

Burg JP, Chen GM (1984) Tectonics and structural zonation of southern Tibet, China. Nature 311(5983):219–223

Byerlee J (1978) Friction of rocks. Pure Appl Geophys 116(4–5):615–626

Davis D, Suppe J, Dahlen FA (1983) Mechanics of fold-and-thrust belts and accretionary wedges. J Geophys Res Solid Earth 88(B2):1153–1172

Davy P, Cobbold PR (1988) Indentation tectonics in nature and experiment. 1. Experiments scaled for gravity. Bull Geol Inst Univ Upps 14:129–141

Dooley TP, Jackson MPA, Hudec MR (2007) Initiation and growth of salt-based thrust belts on passive margins: results from physical models. Basin Res 19(1):165–177

Fielding E, Isacks B, Barazangi M, Duncan C (1994) How flat is tibet? Geology 22:905–908

Godin L, Grujic D, Law RD, Searle MP (2006) Channel flow, ductile extrusion and exhumation in continental collision zones: an introduction. Geol Soc Lond Spec Publ 268:1–23

Grujic D, Warren CJ, Wooden JL (2011) Rapid synconvergent exhumation of miocene-aged lower orogenic crust in the Eastern Himalaya. Lithosphere 3(5):346–366

Hao M, Li Y, Zhuang W (2019) Crustal movement and strain distribution in East Asia revealed by GPS observations. Sci Rep 9(1):16797

Harris N (2007) Channel flow and the Himalayan-Tibetan Orogen: a critical review. J Geol Soc 164(3):511–523

Hodges KV, Parrish RR, Housh TB, Lux DR, Burchfiel BC, Royden LH, Chen Z (1992) Simultaneous miocene extension and shortening in the himalayan orogen. Science 258(5087):1466

Huismans R, Beaumont C (2011) Depth-dependent extension, two-stage breakup and cratonic underplating at rifted margins. Nature 473(7345):74-U85

Jagoutz O, Royden L, Holt AF, Becker TW (2015) Anomalously fast convergence of India and Eurasia caused by double subduction. Nat Geosci 8(6):475–478

Kellett DA, Grujic D, Coutand I, Cottle J, Mukul M (2013) The South Tibetan detachment system facilitates ultra rapid cooling of granulite-facies rocks in Sikkim Himalaya. Tectonics 32(2):252

Kellett DA, Cottle JM, Larson KP (2019) The South Tibetan detachment system: history advances, definition and future directions. Geol Soc Lond Spec Publ 483(1):377–400

Krantz RW (1991) Measurements of friction coefficients and cohesion for faulting and fault reactivation in laboratory models using sand and sand mixtures. Tectonophysics 188(1–2):203–207

Li Z-W, Xu Y, Hao T-Y, Liu J-S, Zhang L (2006) Seismic tomography and velocity structure in the crust and upper mantle around Bohai Sea area. Chin J Geophys 49(3):698–706

Makris J, Papoulia J, Papanikolaou D, Stavrakakis G (2001) Thinned continental crust below northern Evoikos Gulf, central Greece, detected from deep seismic soundings. Tectonophysics 341(1):225–236

Mandal N, Bose S, Baruah A, Sarkar S (2015) First-order topography of the Himalayan Mountain belt: a deep-crustal flow analysis. Geol Soc Lond Spec Publ 412(1):5–23

Martin AJ (2017) A review of definitions of the Himalayan Main Central Thrust. Int J Earth Sci 106(6):2131

Mukherjee S (2013) Channel flow extrusion model to constrain dynamic viscosity and Prandtl number of the higher Himalayan shear zone. Int J Earth Sci 102(7):1811–1835

Mukherjee S (2017) Airy's isostatic model: a proposal for a realistic case. Arab J Geosci 10(268):1–7

Mukherjee S, Koyi H (2010) Higher Himalayan shear zone, Zanskar Indian Himalaya: microstructural studies and extrusion mechanism by a combination of simple shear and channel flow. Int J Earth Sci 99(5):1083–1110

Mukherjee S, Koyi H, Talbot C (2012) Implications of channel flow analogue models for extrusion of the higher Himalayan shear zone with special reference to the out-of-sequence thrusting. Int J Earth Sci 101(1):253–272

Najman Y, Jenks D, Godin L, Boudagher-Fadel M, Millar I, Garzanti E, Horstwood M, Bracciali L (2017) The Tethyan Himalayan detrital record shows that India-Asia terminal collision occurred by 54 Ma in the Western Himalaya. Earth Planet Sci Lett 459(C):301–310

Reber JE, Galland O, Cobbold PR, de Veslud CLC (2013) Experimental study of sheath fold development around a weak inclusion in a mechanically layered matrix. Tectonophysics 586:130–144

Reber JE, Cooke ML, Dooley TP (2020) What model material to use? A review on rock analogs for structural geology and tectonics. Earth Sci Rev 202:1–21

Schmalholz SM, Duretz T, Hetényi G, Medvedev S (2019) Distribution and magnitude of stress due to lateral variation of gravitational potential energy between Indian Lowland and Tibetan Plateau. Geophys J Int 216(2):1313–1333

Searle MP, Simpson RL, Law RD, Parrish RR, Waters DJ (2003) The structural geometry, metamorphic and magmatic evolution of the Everest massif, High Himalaya of Nepal-South Tibet. J Geol Soc 160(3):345

Searle MP, Cottle JM, Streule MJ, Waters DJ (2009) Crustal melt granites and migmatites along the Himalaya: melt source, segregation, transport and granite emplacement mechanisms. Earth Environ Sci Trans R Soc Edinb 100(1–2):219–233

Spicer RA, Harris NBW, Widdowson M, Herman AB, Guo S, Valdes PJ, Wolfe JA, Kelley SP (2003) Constant elevation of southern Tibet over the past 15 million years. Nature 421(6923):622

Talbot C, Aftabi P (2004) Geology and models of salt extrusion at Qum Kuh, central Iran. J Geol Soc 161(2):321–334

ten Grotenhuis SM, Piazolo S, Pakula T, Passchier CW, Bons PD (2002) Are polymers suitable rock analogs? Tectonophysics 350:35–47

Thielicke W, Stamhuis EJ (2014) PIVlab - time-resolved digital particle image velocimetry tool for MATLAB (version: 1.31)

Vendeville BC, Jackson MPA (1992) The rise of diapirs during thin-skinned extension. Mar Pet Geol 9(4):331–354

Weijermars R (1986) Flow behaviour and physical chemistry of bouncing putties and related polymers in view of tectonic laboratory applications. Tectonophysics 124:325–358

Yin A (2006) Cenozoic tectonic evolution of the Himalayan orogen as constrained by along-strike variation of structural geometry, exhumation history, and foreland sedimentation. Earth Sci Rev 76(1):1–131

Zhou H, Luo Z, Zhong B (2014) Qinghai-Tibet Plateau crustal thickness derived from EGM2008 and CRSUT2.0. Geod Geodyn 5(4):9–15